Electronic structure of chromium oxides, CrO_n^- and CrO_n ($n=1-5$) from photoelectron spectroscopy and density functional theory calculations

G. L. Gutsev[a)] and P. Jena
Physics Department, Virginia Commonwealth University, Richmond, Virginia 23284-2000

Hua-Jin Zhai and Lai-Sheng Wang[b)]
Department of Physics, Washington State University, Richland, Washington 99352
and W. R. Wiley Environmental Molecular Sciences Laboratory, Pacific Northwest National Laboratory,
Richland, Washington 99352

The electronic structure of CrO_n^- and CrO_n ($n=1-5$) was investigated using anion photoelectron spectroscopy and density functional theory. Photoelectron spectra of CrO_n^- were obtained at several photon energies and yielded electron affinities, vibrational and electronic structure information about the neutral CrO_n species. Density functional theory calculations were carried out for both the neutrals and anions and were used to interpret the experimental spectra. Several low-lying electronic states of CrO were observed and assigned from photodetachment of the CrO^- ground state ($^6\Sigma^+$) and an excited state ($^4\Pi$), which is only 0.1 eV higher. The main spectral features of CrO_2^- were interpreted based on a C_{2v} CrO_2^- ($^4B_1$). A very weak $Cr(O_2)^-$ isomer was also observed with lower electron binding energies. Relatively simple and vibrationally resolved spectra were observed for CrO_3^-, which was determined to be D_{3h}. The CrO_3 neutral was calculated to be C_{3v} with the Cr atom slightly out of the plane of the three O atoms. The spectrum of CrO_4^- revealed a very high electron binding energy. Several isomers of CrO_4^- were predicted and the ground state has a distorted tetrahedral structure (C_2) without any O–O bonding. Only one stable structure was predicted for CrO_5^- with a superoxo O_2 bonded to a C_{3v} CrO_3. © *2001 American Institute of Physics.* [DOI: 10.1063/1.1405438]

I. INTRODUCTION

Transition metal (TM) oxides are technologically important materials and have numerous applications, such as catalysts in conversion processes of hydrocarbons.[1,2] These materials exhibit different stoichiometries due to the existence of various oxidation states of the TM metals. Oxides of chromium, in particular, are widely used as coating materials in magnetic recording devices.[3,4] It was found that properties of these devices depend strongly on the stoichiometry of the chromium oxides. Investigations of the structural and electronic properties of TM oxide clusters with different metal to oxygen ratios help to understand the physical and chemical properties of the bulk materials and provide valuable insights into their perspective applications. In the present article, we report an investigation of the simplest chromium oxide species, CrO_n^- and CrO_n ($n=1-5$), using anion photoelectron spectroscopy (PES) and density functional theory (DFT) calculations.

Among the small CrO_n species, chromium trioxide shows a very high electron affinity (EA), which indicates that it should be a strong oxidizing agent.[5] Species with large EA's have the ability to trap free electrons in excited gases and form extremely stable negative ions. Accurate EA values of the CrO_n species can also be used for an improvement of thermodynamic data, but they have been difficult to obtain. For example, the EA values of CrO_3 deduced from previous thermodynamic methods vary widely from 3.16 to 4.05 eV.[6] On the other hand, PES, applied previously to many *3d* TM oxide clusters in our laboratory and Lineberger's group,[7–19] is based on direct measurements of the electron detachment energies and allows more precise EA determinations. Since PES of anions reflects transitions from anion states to the corresponding neutral states, it provides information on the electronic structure of both the anions and their neutral parents. In our recent study of MnO_n^-,[14] we found that theoretical calculations are very helpful in the interpretation of the photoelectron spectra, as well as in understanding the electronic and geometrical structures of both the anions and the neutral species. A similar approach is applied here to the CrO_n^- series, especially for $n=3-5$, for which there is little previous work.

Among the *3d* TM oxide anions, theoretical studies have been performed for ScO_2^-,[20–22] TiO_n^-,[23] VO_n^-,[24] MnO_n^-,[14,25,26] and FeO_n^-[27,28] and good agreement between experimental data and the calculated EA's of the corresponding neutral species has generally been obtained. Detailed studies of the electronic and geometrical structure of the neutral and anionic *3d* TM monoxides[29] and dioxides[30] have been performed using DFT methods with different generalized gradient approximations for the exchange-correlation functional. These studies showed that the BPW91 approach (an abbreviation for a combination of Becke's exchange[31]

and Perdew–Wangs' correlation[32] functionals) provides similar results as the BLYP one (Becke's exchange[31] and Lee–Yang–Parr correlation[33]), which are generally superior to those obtained by a hybrid Hartree–Fock–DFT B3LYP approach.[34]

The current work is aimed at understanding the electronic and geometrical structures of the monochromium oxide species CrO_n and CrO_n^- ($n = 1-5$) using a combined experimental and theoretical study. Among these five oxide species, CrO^- and CrO_2^- have been previously studied by PES at a lower photon energy.[15,16] Several photon energies are used in the current work because higher photon energies are necessary for oxygen-rich species, which generally have very high EA's. Geometrical structures for both the neutral and negatively charged clusters are optimized at the BPW91 level. Electron detachment energies were also calculated from the anions and were used to help interpret the experimental PES data.

II. EXPERIMENTAL AND COMPUTATIONAL DETAILS

A. Experimental method

Our experiments were performed with a magnetic bottle time-of-flight photoelectron spectrometer, which has been described in detail elsewhere.[35,36] The apparatus is composed of a laser vaporization source, a time-of-flight mass spectrometer and a magnetic bottle time-of-flight electron analyzer. Chromium atoms, generated from laser vaporization of a pure Cr target, reacted with O_2 seeded in a helium carrier gas, producing a series of oxide clusters. The clusters entrained in the carrier gas underwent a supersonic expansion and collimated by a skimmer. Anions from the collimated beam were extracted perpendicularly into a time-of-flight mass analyzer. Desired anions were mass-selected and subsequently decelerated before crossing a detachment laser beam. Both a Q-switched Nd:YAG laser (532 nm–2.331 eV, 355 nm–3.496 eV, and 266 nm–4.661 eV) and an ArF excimer laser were used for photodetachment in the current experiments. The energy resolution of our apparatus was better than 30 meV for 1 eV electrons, as calibrated with Cu^-. Due to the dependence of the resolution on electron kinetic energies, lower photon energy spectra yielded better resolved data. But high photon energies were necessary to investigate species with high EA's, as well as yielding more excited states of the neutral species.

B. Theoretical procedures

Our calculations were performed using an approach where linear combinations of atomic orbitals constitute one-electron molecular orbitals (MO-LCAO). The many-electron potential was constructed using DFT with a generalized gradient approximation for the exchange-correlation functional. A combination of Becke's exchange[31] and Perdew–Wangs' correlation[32] functionals, referred to as BPW91, was used as implemented in GAUSSIAN 94.[37] For the atomic orbitals, we used the standard 6-311+G* basis (Cr:[$15s11p4d1f/10s7p4d1f$] and O:[$13s6p1d/5s4p1d$]) due to Wachters and Hay.[38,39] Geometry optimizations were carried out by the steepest descent method until the gradient forces fell below

the threshold value of 3×10^{-4} au. Analytical harmonic frequency calculations were performed subsequently to confirm that the optimized geometrical configurations corresponded to stationary states.

Density functional theory is valid for the lowest energy states in each particular (spatial and spin) symmetry.[40–43] Extensive optimizations, beginning with different spatial configurations for each spin multiplicity for both the CrO_n and CrO_n^- series, were performed to ensure that the ground-state configurations were identified unambiguously. Comparison of the computed properties with experimental data was made to further verify our theoretical results. Vertical binding energies ($E_{b,i}$) or vertical detachment energies (VDE's), which correspond to band maxima in photodetachment spectra, are due to a sudden detachment of an electron from an anion (A) to the corresponding neutral parent in some particular state N_i. The quantity $E_{b,i}$ can be evaluated at the equilibrium ground-state geometry R_A of the anion as:

$$E_{b,i} = E_{tot}(N_i, R_A) - E_{tot}(A, R_A). \tag{1}$$

With the present approach, only two transitions to neutral states N_k ($k = 1$ and 2) can be computed directly. If the ground-state spin multiplicity of the anion is $2S + 1 = M$, then we can compute the energies of electron detachment resulting in the two lowest neutral states with spin multiplicities $2S + 1 = M \pm 1$.

In order to evaluate transition energies to other neutral states, one could apply an approximate formula, which we used to assign features in the PES spectra of the MnO_n^- anions,[14]

$$E_{b,j} = E_{tot}(N_{kn}, R_A) - E_{tot}(A, R_A) + (\varepsilon_{HOMO,n}^A - \varepsilon_{j,n}^A), \tag{2}$$

where $k(=1$ or $2)$ denotes the neutral states accessible from the anion ground state as in Eq. (1), $j > 2$, n (α or β) denotes the spin representation, and $\varepsilon_{j,n}^A$ are eigenvalues to the Kohn–Sham orbitals of the anion ground state, $\varepsilon_{HOMO,n}^A$ is the eigenvalue to the highest occupied molecular orbital in the n spin representation.

Adiabatic detachment energies (A_{ad}), corresponding to removal of an electron from the ground state of the anion to states of the neutral at their respective equilibrium geometries, are given by the differences in total energies of the neutral and anion states:

$$A_{ad} = E_{tot}(N, R_N) + Z_N - E_{tot}(A, R_A) - Z_A = \Delta E_{el} + \Delta E_{nuc}, \tag{3}$$

where R_N and R_A denote ground-state equilibrium geometries of a neutral molecule (N) and its anion (A), respectively. Zero-point energies (Z) were computed within the harmonic approximation. While values of $E_{b,i}$ correspond to band maxima in a PES spectrum, the A_{ad} values are to be deduced from the thresholds of PES bands or the 0–0 transitions of vibrationally resolved bands. The A_{ad} Value obtained for the ground-state transition corresponds to the EA of the neutral molecule. Electron affinity measures the total energy gain of a system due to attachment of an extra electron and represents an important thermodynamic quantity.
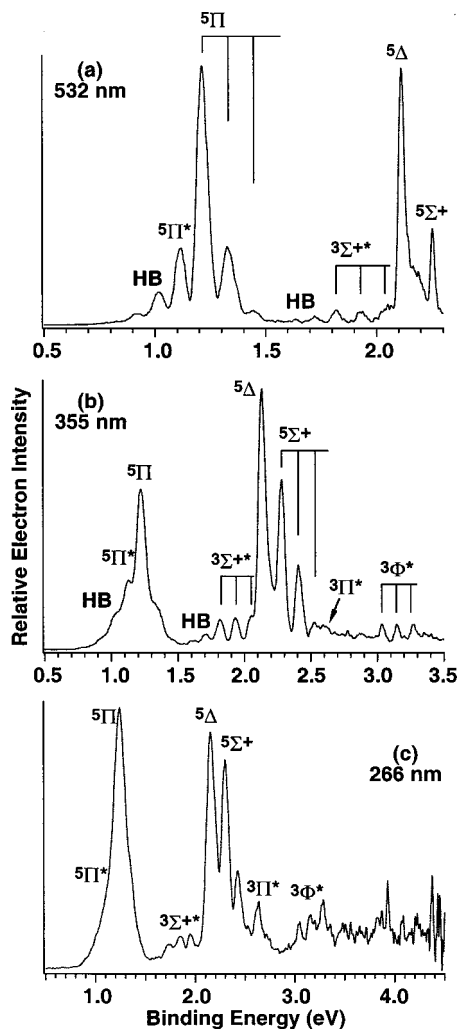
J. Chem. Phys., Vol. 115, No. 17, 1 November 2001

Electronic structure of chromium oxides   7937

FIG. 1. Photoelectron spectra of CrO^- at (a) 532 nm (2.331 eV), (b) 355 nm (3.496 eV), and (c) 266 nm (4.661 eV). HB stands for hot bands. * indicates transitions from an excited state of CrO^-.

In order to estimate the thermodynamic stability of the chromium oxides, we also computed fragmentation energies as the differences in total energies of fragments F_i formed in a particular decay channel and the total energy of an initial compound M:

$$D_e(M) = \sum_i E_{tot}(F_i) - E_{tot}(M), \qquad (4)$$

where the zero-point energy corrections are neglected because they are relatively small.

III. EXPERIMENTAL AND THEORETICAL RESULTS

A. Experimental results

Figure 1 shows the spectra of CrO^- measured at three photon energies. Well-resolved bands with vibrational structures were obtained. Many excited-state features were observed in the 266 nm spectrum [Fig. 1(c)], but they could not be clearly resolved and assigned beyond ~3.5 eV owing to limited resolution and spectral congestion. A high resolution spectrum of CrO^- obtained at 351 nm was reported previously by Lineberger *et al.*,[15] but no detailed assignment was

given. Generally, the current data agree well with the previous high resolution spectrum, with minor variations in relative intensities, due to the different experimental techniques employed (the current experiment is angle-integrated and measures electrons from all 4π solid angles). In particular, the 2.13 eV feature ($^5\Delta$) is much stronger than the previous spectrum, whereas the 1.82 eV vibrational progression ($^3\Sigma^+*$) appears to be weaker but with stronger hot band transitions (HB). Two more additional and relatively weak features could also be identified from the current spectra at 355 and 266 nm: the feature at 2.64 eV ($^3\Pi*$) whose intensity was enhanced in the 266 nm spectrum and a vibrational progression starting at 3.03 eV ($^3\Phi*$). More transitions were observed in the 266 nm [Fig. 1(c)], but could not be definitely identified due to limited spectral resolution and congestion. The assignments were made on the basis of our theoretical calculations, as discussed later. The observed states are labeled in Fig. 1 (* indicates transitions from an excited anion) and compared with the theoretical calculations in Table I. The observed detachment transitions and obtained spectroscopic constants are given in Fig. 2.

The spectra of CrO_2^-, shown in Fig. 3, were obtained at three detachment energies as well. The 355 nm spectrum [Fig. 3(a)] was vibrationally resolved with the 0–0 transition at 2.43 eV. There appears to be two vibrational progressions. The main progression has a vibrational spacing of about 900 cm^{-1}, and the other progression has a spacing of about 220 cm^{-1}. Very weak signals (X′) were observed at ~1.5 eV. These signals completely disappeared when the carrier gas was seeded with N_2O, instead of O_2, as was the case for the 193 nm spectrum [Fig. 3(c)]. The weak features were likely due to a $Cr(O_2)^-$ isomer, as discussed later. The 266 nm spectrum [Fig. 3(b)] revealed two more intense features (A and B), compared to the 355 nm spectrum. The broadness of these features indicates that there must be significant geometry changes between the anions and the corresponding neutral states or there might be overlapping and unresolved electronic transitions. At 193 nm, there seemed to be unresolved features throughout the higher energy side beyond feature B. The relative intensities of the first three detachment bands in the 193 nm spectrum were changed compared to the 266 nm spectrum.

The weak low-binding energy feature around 1.5 eV completely disappeared in the 193 nm spectrum because an N_2O-seeded He carrier gas was used in this experiment. Similar behavior was observed in the 266 and 355 nm spectra taken under the same conditions. This feature is likely due to a peroxo species $Cr(O_2)^-$, which is consistent with the results of our previous DFT calculations performed for oxo, peroxo, and superoxo isomers of chromium dioxide and its anion.[30] The low EA of this isomer is also in agreement with a general anticipation that a $3d$-metal oxygen peroxo complex $M(O_2)$ has a lower EA than the corresponding $3d$-metal oxo complex OMO.[7] A higher resolution spectrum of CrO_2^- obtained at 351 nm was previously reported by Lineberger *et al.*[16] However, the 351 nm photon energy allowed only the first detachment band to be observed. The current spectrum at 355 nm is consistent with the previous data, although the previous spectrum showed a much broader

TABLE I. Experimental (Expt.) and calculated vertical electron detachment energies (eV) from the two lowest-lying states of CrO⁻.

Electron configuration	Final state	BPW91 6-311+G*	BPW91 Augmen.[a]	BLYP 6-311+G*	BLYP Augmen.[a]	Expt.
$CrO^-(^6\Sigma^+)9\sigma^1 1\delta^2 4\pi^2$						
$\rightarrow 9\sigma^1 1\delta^2 4\pi^1$	$^5\Pi$	1.22	1.24	1.06	1.11	1.22±0.01
$\rightarrow 9\sigma^1 1\delta^1 4\pi^2$	$^5\Delta$	2.17	2.22	1.93	2.02	2.13±0.02
$\rightarrow 9\sigma^0 1\delta^2 4\pi^2$	$^5\Sigma^+$	2.47	2.41	2.23	2.20	2.28±0.03
$\rightarrow 3\pi^3 9\sigma^1 1\delta^2 4\pi^2$	$^7\Pi$	3.84	3.89	3.69	3.79	
	$^5\Pi$	4.54	4.56	4.24	4.32	
$\rightarrow 8\sigma^1 9\sigma^1 1\delta^2 4\pi^2$	$^7\Sigma^+$	4.49	4.52	4.34	4.41	
	$^5\Sigma^+$	4.89	4.91	4.62	4.70	
$CrO^-(^4\Pi)9\sigma^2 1\delta^2 4\pi^1$		+0.31[b]	+0.34[b]	−0.05[b]	−0.003[b]	+0.096[b]
$\rightarrow 9\sigma^1 1\delta^2 4\pi^1$	$^5\Pi$	0.87	0.86	1.06	1.08	1.12±0.01
$\rightarrow 9\sigma^2 1\delta^2 4\pi^0$	$^3\Sigma^+$	1.97	1.97	1.81	1.83	1.82±0.02
$\rightarrow 9\sigma^1 1\delta^2 4\pi^1$	$^3\Pi$	2.65	2.62	2.38	2.37	2.64±0.03
$\rightarrow 9\sigma^2 1\delta^1 4\pi^1$	$^3\Phi$ or $^3\Pi$	3.22	3.21	2.93	2.94	3.03±0.03
$\rightarrow 8\sigma^1 9\sigma^2 1\delta^2 4\pi^1$	$^5\Pi$	4.16	4.21	4.22	4.26	
$\rightarrow 3\pi^3 9\sigma^2 1\delta^2 4\pi^1$	$^5\Sigma^-$	4.83	4.87	4.87	4.90	

[a]Basis Cr[$19s13p11d6f$] is obtained by adding exponents intermediate between those of the standard 6-311+G* basis and five diffuse f-functions. For O, the standard 6-311+G($3df$) basis is used.
[b]Energy in eV relative to the $^6\Sigma^+$ state.

Franck–Condon envelope for the X band, apparently due to intense hot band transitions.

Figure 4 shows the spectra of CrO_3^- taken at two photon energies. The 266 nm spectrum [Fig. 4(a)] exhibited a well-resolved vibrational progression with an average spacing of 890 cm⁻¹. Two more well-separated and well-resolved bands (A and B) were observed in the 193 nm spectrum [Fig. 4(b)]. The weak features might be due to vibrational structures or possible overlapping transitions as revealed from our theoretical results. The weak feature *a* to the left of the *A* feature was due to a discrete detachment transition. As discussed later, several transitions might have contributed to the *B* feature.
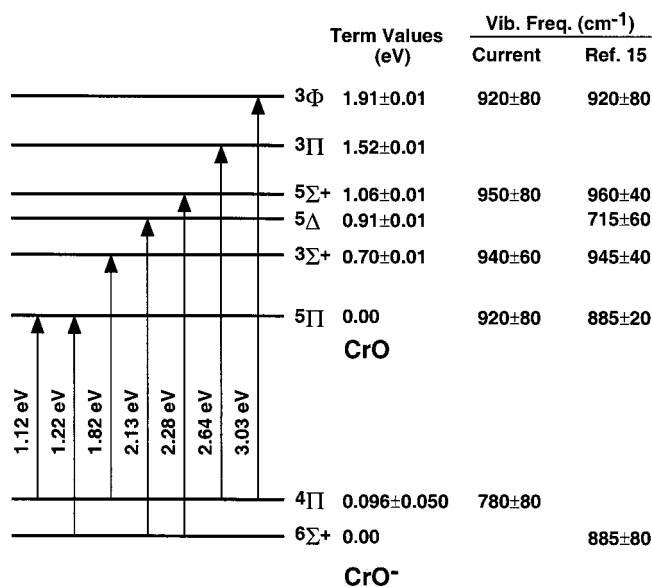
Both CrO_4^- and CrO_5^- were found to have very high electron detachment energies and their spectra could only be observed at 193 nm, as shown in Fig. 5. Two well-resolved and intense features were observed for CrO_4^- [Fig. 5(a)]. There were also weak features tailing the lower energy side

FIG. 2. The observed detachment transitions from the two anionic states of CrO⁻ and the spectroscopic constants of CrO.
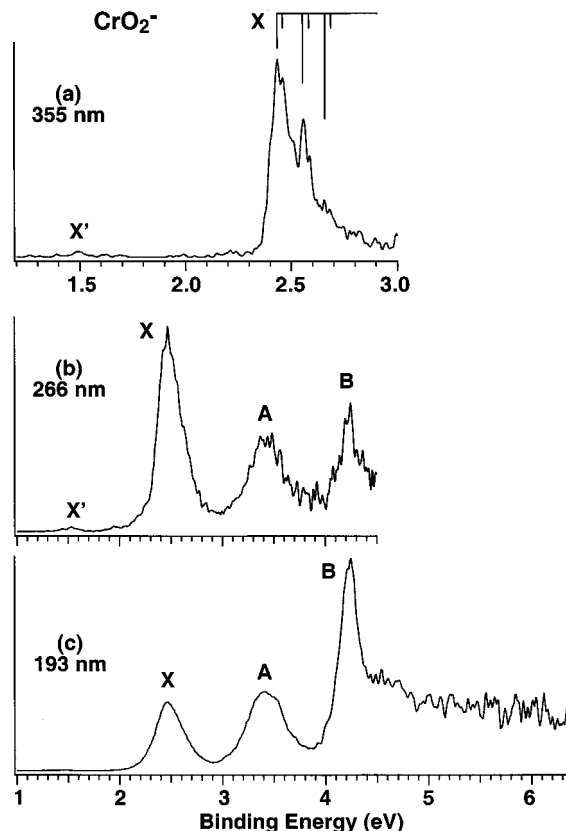
FIG. 3. Photoelectron spectra of CrO_2^- at (a) 355 nm, (b) 266 nm, and (c) 193 nm (6.424 eV). The vertical lines in (a) indicate resolved vibrational progressions.
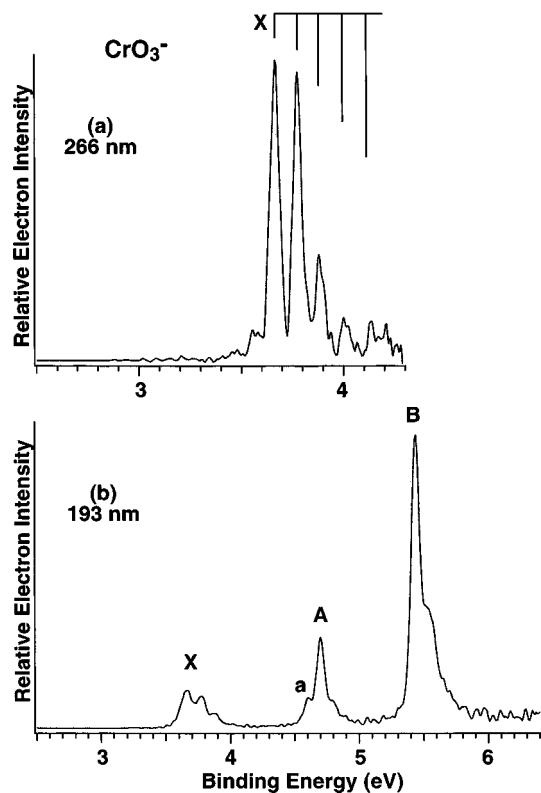
FIG. 4. Photoelectron spectra of CrO_3^- at (a) 266 nm and (b) 193 nm. The vertical lines in (a) indicate the resolved vibrational progression.

TABLE II. Observed vertical electron detachment energies (VDE) and spectroscopic constants for CrO_n and CrO_n^- ($n=2-5$) compared with theoretical results (Theor.) computed according to Eqs. (1) and (2).

| | | VDE (eV)[a] | | Vib. freq.[a] |
	State	Expt.	Theor.[b]	(cm^{-1})
$Cr(O_2)$	X^5B_2	1.50(6)	1.37	
CrO_2	X^3B_1	2.43(2)	2.35	900(80)[c]; 220(40)[d]
	A^3A_1, $^3B_1$	3.41(5)	2.73	
	B^5A_2, $^3A_2$	4.25(5)	4.26	
	$^5A_1$, $^3B_1$, $^5B_1$	>4.5	4.66	
CrO_3[e]	X^1A_1'	3.66(2)	3.61	890(60)
	a^1A_2'	4.61(2)	4.42	
	A^3A_1'	4.70(2)	4.61	
	$^1A_2''$, $^3A_2''$	5.43(2)	5.57, 5.75	
CrO_4	X^3A_2	5.07(4)	4.95	
	A^1A	6.04(3)	6.13	
CrO_5	X^3A''	4.7(1)	4.69	
	A^1A'	5.33(4)	5.17	

[a]The numbers in the parentheses represent uncertainties in the last digits.
[b]Theoretical data for CrO_2 are from Ref. 30.
[c]The symmetric stretching mode (ν_1).
[d]The bending mode (ν_2).
[e]Final states are labeled according to the D_{3h} point group of the CrO_3^- anion.

fact due to direct detachment transitions. The spectrum of CrO_5^- revealed a very broad band (X) at lower binding energies and two features (A and B) at higher binding energies. Our experimental results for CrO_n^- ($n=2-5$) are summarized in Table II and compared to our theoretical results, as discussed below.

of the X band and between the X and A bands. The low-energy tail could be due to minor isomers presented in the anion beam. As shown later from our theoretical calculations, the weak features between the X and A bands were in
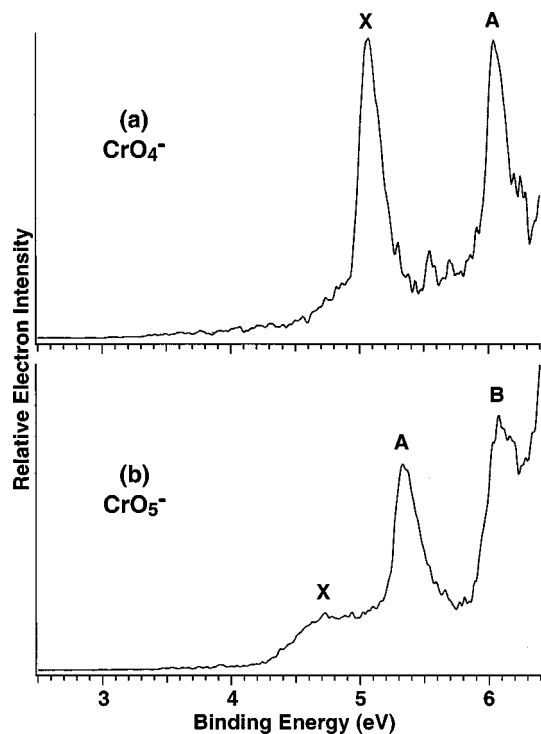
B. Theoretical results

Optimized ground-state geometries of CrO, CrO_2, CrO_3, and CrO_5 and their anions are presented in Fig. 6. Many low-lying isomers and excited states of CrO_4 and CrO_4^- are found and are shown in Fig. 7. Theoretical investigations of CrO_2^- with several isomers were reported in more detail previously,[30] and Fig. 6 only displays the oxo ground state for CrO_2 ($^3B_1$) and CrO_2^- ($^4B_1$). The structures of low-lying

FIG. 5. Photoelectron spectra of (a) CrO_4^- and (b) CrO_5^- at 193 nm.
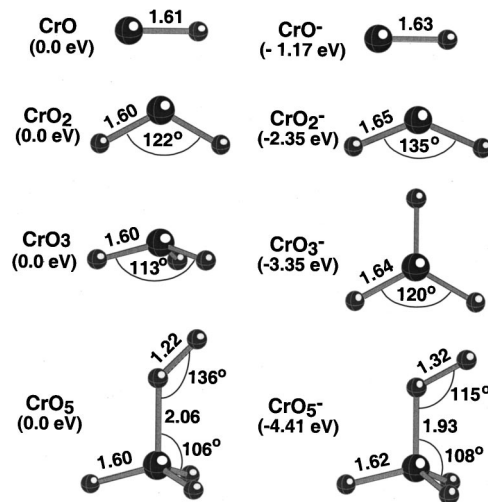

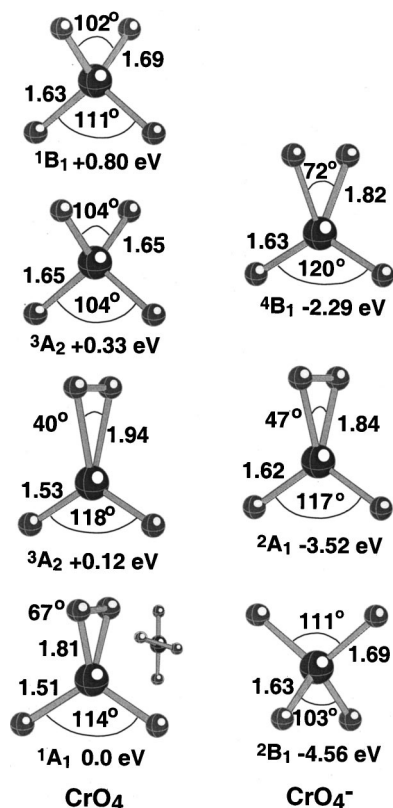FIG. 6. Ground-state geometrical configurations of CrO, CrO_2, CrO_3, and CrO_5 along with their anions.

FIG. 7. Geometric configurations of the ground and lowest excited states of CrO_4 and CrO_4^-.

peroxo and superoxo isomers of CrO_2 and CrO_2^- are not shown. In the current theoretical work, we focus on the monoxide and the higher oxides starting with CrO_3.

The ground state of CrO_3 ($^1A_1$) is closed shell with C_{3v} symmetry and an out-of-plane angle of 15.6° (Fig. 6). Previous calculations using a local-spin-density-approximation (LSDA) approach and the LSDA with nonlocal corrections (NLSDA)[44] yielded similar geometric structures with the Cr–O bond length being 1.59 and 1.62 Å at the LSDA and NLSDA levels, respectively. Our computed harmonic frequency for the symmetric stretching mode (a_1) of 959.6 cm^{-1} is in good agreement with the value of 890 cm^{-1} measured from the PES spectrum of CrO_3^- (Table II). A value of 968.4 cm^{-1} was obtained for this mode by Andrews *et al.*[45] from infrared spectra of CrO_3 trapped in inert matrices. The lowest-energy isomers of CrO_3 were found to be well-separated in total energy from the ground state: a triplet oxo state ($^3A_2$) by 1.22 eV and a singlet peroxo state ($^1A_1$) by 3.15 eV. The ground state of CrO_3^- has D_{3h} symmetry with a $^2A_1'$ electronic state. This state is quite floppy and its out-of-plane vibrational mode (a_2'') is only 43 cm^{-1}, indicating a rather flat potential-energy curve for the out-of-plane motion. We did not find any stable isomer for CrO_3^- below the detachment continuum, consistent with the experiment (Fig. 4), where, unlike the other oxides, no trace of isomers was observed.

For both CrO_4 and CrO_4^-, we found several stable isomers closely spaced in energy (Fig. 7). The ground state of neutral CrO_4 has a rather unusual geometrical shape: it has

C_2 symmetry with two opposite pairs of oxygen atoms slightly rotated around the C_2 axis (Fig. 7). The upper ∠OCrO bond angle is 67°, which is intermediate between typical values of peroxo (40°–45°) and oxo (100°–120°) bond angles. A peroxo isomer is higher in energy by only 0.12 eV. The CrO_4^- anion has at least three states, which are stable thermodynamically relative to detachment of the extra electron. The ground state of CrO_4^- is $^2B_1$ and has an oxo form of C_{2v} symmetry. This geometrical configuration is similar to the isoelectronic MnO_4.[25] A peroxo doublet ($^2A_1$) and a half-peroxo quartet ($^4B_1$) isomer of CrO_4^- were found to be above the ground state by 1.04 and 2.27 eV, respectively.

An extensive search for a thermodynamically stable state of CrO_5 resulted in only one configuration ($^3A''$) of the superoxo type, as shown in Fig. 6. The ground state ($^2A''$) of the CrO_5^- anion has the same superoxo shape and is below the ground state of the neutral parent by 4.41 eV. We found another isomer for CrO_5^-, which also has a doublet spin multiplicity with a double peroxo geometrical shape. This isomer is above the ground state anion by 1.81 eV.

IV. DISCUSSION AND COMPARISONS OF EXPERIMENTAL AND THEORETICAL RESULTS

A. CrO and CrO⁻

The ground state of CrO is known to be $^5\Pi$ with an electron configuration, $1\delta^2 4\pi^1 9\sigma^1$.[46,47] Upon formation of the anion, the extra electron can enter either the 9σ MO to give a $^4\Pi$ state or the 4π MO to give a $^6\Sigma^+$ state. Our theoretical results, as given in Table I, suggest that the two states are nearly degenerate in total energy. Direct computations of VDE's from the two anions to the neutral CrO ground state were performed according to Eq. (1) and VDE's to excited states of CrO were computed according to Eq. (2). Our results obtained at the BPW91 and BLYP levels of theory with the use of two basis sets (the 6-311+G* basis and an augmented 6-311+G* one), are given in Table I. The variations at the different levels of theory are rather small and the ordering of the energy levels obtained is consistent.

The strong peak at 1.22 eV is assigned to be the transition from the ground state of the anion to the ground state of the neutral. This assignment is consistent with that of Lineberger *et al.*[15] The obtained EA is also in excellent agreement with the previous value of 1.221 eV. The peaks at lower binding energies appeared as hot band transitions. However, as was pointed out previously by Lineberger *et al.*,[15] the peak at 1.12 eV is too intense to be due to a hot band transition. It was assigned to be from an excited state of the anion. Comparing the current spectra to that of Lineberger *et al.*, we note that the excited anion state was even more populated in the current experiment. The observation of excited anions was consistent with our theoretical results, which indicated that there are two nearly degenerate anion states depending on which orbitals the extra electron enters. Experimentally, the two anionic states differ by 0.096 eV, according to the above assignment. Such a small energy difference could not be definitively distinguished at the current levels of theory, as one can see from Table I. Lineberger

et al. assumed that the ground state of CrO$^-$ was $^4\Pi$, but did not provide any spectral assignments.

The two strongest excited-state transitions correspond to the feature at 2.13 eV and the vibrational progression starting at 2.28 eV. The binding energies of these two states are in good agreement with the computed vertical binding energies for the $^5\Delta$ and $^5\Sigma^+$ states from the $^6\Sigma^+$ anion, respectively, as shown in Table I. The features observed at 1.82, 2.64, and 3.03 eV are in good agreement with the three low-lying states derived from the $^4\Pi$ state of the anion (Table I). The weak intensities of these transitions suggested that they are more likely to be from the excited anion. Thus, the combined experimental and theoretical results allowed us to conclude that the $^6\Sigma^+$ state should be the ground state of the anion. Figure 2 shows the spectroscopic transitions and the obtained spectroscopic constants. The more accurate vibrational frequencies for the corresponding transitions observed by Lineberger *et al.* are also given in Fig. 2.

The vibrational frequency (ω_e) of CrO computed[29] at various levels of theory is 911 cm^{-1} (BPW91), 903 cm^{-1} (BLYP), and 870 cm^{-1} (B3LYP), which are all in good agreement with the average vibrational spacing of 920 cm^{-1} obtained from the present spectra, as well as with the previous more accurate gas-phase experimental value[46] of 898 cm^{-1}. Theoretical frequencies[29] were also computed for the two anionic states: 827 cm^{-1} (BPW91), 810 cm^{-1} (BLYP), and 815 cm^{-1} (B3LYP) for $^6\Sigma^+$ and 879 cm^{-1} (BPW91), 876 cm^{-1} (BLYP), and 861 cm^{-1} (B3LYP) for $^4\Pi$. The latter are also in reasonable agreement with the experimental value of 780 ± 80 cm^{-1}.

B. CrO$_2$ and CrO$_2^-$

The ground state of CrO$_2^-$ has a C_{2v} structure and a quartet electronic state ($^4B_1$) with an electronic configuration, $9a_1^2 3b_1^2 6b_2^2 10a_1^1 4b_1^1 11a_1^1$. Detachment of the electron from the $11a_1$ HOMO leads to neutral CrO$_2$ in its ground state ($^3B_1$) with an electronic configuration, $9a_1^2 3b_1^2 6b_2^2 10a_1^1 4b_1^1$. The VDE corresponding to this process computed according to Eq. (1) is 2.35 eV, which is in good agreement with the first PES feature (X) of CrO$_2^-$ at 2.43 eV (Fig. 3, Table II). Although both the ground states of CrO$_2^-$ and CrO$_2$ have C_{2v} symmetry, the neutral has a shorter Cr–O bond length and smaller $\angle$O–Cr–O angle, as shown in Fig. 6. These geometry changes between the anion and the neutral are consistent with the PES spectrum [Fig. 3(a)], which revealed vibrational excitations in two modes. The 900 cm^{-1} mode should be due to the Cr–O symmetric stretching and the 220 cm^{-1} mode the bending mode. These vibrational frequencies and assignments are consistent with those by Lineberger *et al.*[16]

The second direct computation of the detachment energy corresponds to removal of an electron from the $6b_2^\beta$ MO [the topmost MO in the β (minority) spin representation] and yielded a VDE of 4.26 eV, which corresponds to the vertical detachment to a $^5A_2$ final neutral state. This computed VDE value is in excellent agreement with the VDE of the B band (4.25 eV) in the PES spectra (Fig. 3). Applying Eq. (2), we estimated approximate detachment energies from other va-

lent MOs as given in Table II. It was found that the VDE's for detachment from the $4b_1(^3A_1)$ and $10a_1(^3B_1)$ orbitals are very close (~2.73 eV) and they were assigned to correspond to the broad feature A observed around 3.4 eV. The 193 nm spectrum showed almost continuous signals above feature B, consistent with the presence of many closely spaced transitions due to detachments of electrons from the inner valent orbitals.

C. CrO$_3$ and CrO$_3^-$

The ground state of neutral CrO$_3$ has C_{3v} symmetry (Fig. 6) with a closed-shell electronic configuration, $9a_1^2 7e^4 1a_2^2 (10a_1)^0$ corresponding to a $^1A_1$ state, whereas the CrO$_3^-$ anion has D_{3h} symmetry and an electronic configuration $(1e'')^4 (3a_2'')^2 (6e')^4 (1a_2')^2 (7a_1')^1$ which corresponds to a $^2A_1'$ state. Direct computations of detachment energies according to Eq. (1) to the singlet and triplet states provide values of 3.61 and 4.61 eV, respectively, in excellent agreement with the first two PES features at 3.66 eV (X) and 4.70 eV (A) (Fig. 4). The triplet neutral state (at the equilibrium anion geometry) has the electronic configuration $\ldots (1a_2')^1 (7a_1')^1$, which could be identified as corresponding to a $^3A_2$ state of the neutral after the geometry relaxation takes place. The latter state is the lowest in total energy among the optimized triplet states of neutral CrO$_3$ and is above the ground $^1A_1$ state by 1.22 eV. The broad vibrational progression observed for the X band indicates that there is a large geometry change between the ground states of the anion and the neutral. The 890 cm^{-1} vibrational spacing is in reasonable agreement with the calculated symmetric stretching frequency of 959.6 cm^{-1}. The bond length change between the anion and the neutral ground state (Fig. 6) is also consistent with the observed vibrational progression. The change from D_{3h} CrO$_3^-$ to C_{3v} CrO$_3$ suggests that the out-of-plane bending mode should also be active in the X band. However, our calculations gave a very low bending frequency (43 cm^{-1}), which is too small to be resolved under our current experimental conditions.

Using Eq. (2) with two reference energies $[E_{tot}(A,^1A_1') - E_{tot}(A,^2A_1')] = 3.61$ eV and $[E_{tot}(A,^3A_2') - E_{tot}(A,^2A_1')] = 4.61$ eV, we obtained a set of energies corresponding to detachment of an electron with subsequent formation of singlet and triplet states: 4.42 eV ($^1A_2'$), 5.18 eV ($^1E'$), 5.57 eV ($^1A_2''$), 5.33 eV ($^3E'$), and 5.75 eV ($^3A_2''$). Such closely spaced energies are related to the nearly same orbital energies in both majority and minority spin representations. The 4.42 eV transition ($^1A_2'$) may correspond to the feature labeled a at 4.61 eV [Fig. 4(b)]. The third main detachment feature labeled B may then be due to detachment from the $6e'$ and $3a_2''$ orbitals, corresponding to the last four calculated detachment transitions. The large intensity of feature B is consistent with the overlapping nature of the assigned transitions. The detachment from the $1e''$ MO was computed to occur at 6.68 eV, which is beyond the 193 nm photon energy, consistent with our PES spectra. However, all the latter assignments can only be viewed as tentative. With our current one-electron approach, it is difficult to reach a quantitative assignment. Multireference theoretical models would be re-

TABLE III. Experimental and theoretical adiabatic electron affinities (eV) for CrO_n ($n = 1-5$).

	CrO	CrO$_2$	Cr(O$_2$)	CrO$_3$	CrO$_4$	CrO$_5$
Expt.	1.22±0.01[a]	2.43±0.02[b]	1.50±0.06	3.66±0.02	4.98±0.09	4.4±0.1
Theor.	1.17	2.22	1.37	3.38	4.61	4.41

[a]1.221±0.006 eV from Ref. 15.
[b]2.413±0.008 eV from Ref. 16.

quired to pin down the excited states of the CrO$_3$ neutral species. The seeming simplicity of the CrO$_3^-$ PES spectra may in fact contain complicated and overlapping detachment transitions.

D. CrO$_4$ and CrO$_4^-$

The ground state of CrO$_4$ is ^1A (C_2 symmetry) and its electronic configuration is $15a^2 13b^2$. But there are two low-lying triplet states, as shown in Fig. 7. The triplet peroxo state is only 0.12 eV above the ground state CrO$_4$. The anion ground state has an electronic configuration of $13a_1^2 2a_2^2 7b_2^2 7b_1^1$, corresponding to a $^2B_1$ (C_{2v}) state, which is degenerate in total energy with a $^2B_2$ state. Detachment from the $7b_1$ MO results in the neutral $^1A_1$ ground state with $[E_{tot}(A,^1A_1) - E_{tot}(A,^2B_1)] = 6.13$ eV, whereas detachment from $7b_2$ leads to a $^3A_2$ state with $[E_{tot}(A,^3A_2) - E_{tot}(A,^2B_1)] = 4.95$ eV, which is slightly above the peroxo $^3A_2$ state, the lowest triplet state of the neutral (Fig. 7). These two detachment channels are in excellent agreement with the two main PES features at 5.07 eV (X) and 6.04 eV (A). Here, we met the case where the first vertical detachment of an extra electron from the singly occupied MO results in formation of a neutral at C_{2v} symmetry, which would relax to C_2 symmetry. This is a really unusual situation: this first transition to the singlet ^1A state has an energy higher by 1.2 eV than the transition to the triplet $^3A_2$ state, which is higher in total energy but has a similar geometry as the anion. This suggests that the A band corresponding to removal of the $7b_1$ electron should have a long low-energy tail extending to the left of the X band, not inconsistent with our PES spectrum [Fig. 5(a)]. Using Eq. (2) with two reference energies, we estimated energies of several other vertical transitions. The estimated singlet states are: 5.29 eV ($^1A_2$), 5.60 eV ($^1B_2$), 6.53 eV ($^1A_2$), and 6.71 eV ($^1B_1$); and the triplet states are: 5.03 eV ($^3B_2$), 6.06 eV ($^3B_1$), and 6.09 eV ($^3A_2$). All these transitions except the 6.53 and 6.71 singlet states may be contained in the PES spectrum of CrO$_4^-$ [Fig. 5(a)].

E. CrO$_5$ and CrO$_5^-$

We found CrO$_5$ to possess only one thermodynamically stable state of a superoxo type (C_s) with a triplet state $^3A''$ $[(8a'')^2(22a')^2(9a'')^2(23a')^1(10a'')^1]$. The ground state of the CrO$_5^-$ anion is $^2A''[\ldots(23a')^2(10a'')^1]$ and has a similar C_s geometrical shape as its neutral parent, as shown in Fig. 6. According to Eq. (1), detachment of an electron from the $23a'$ orbital results in the $^3A''$ neutral ground state with a VDE of 4.69 eV, whereas detachment from the $10a''$ orbital reaches a dissociative $^1A'$ neutral state with a VDE of 5.17 eV. These two computed detachment channels are in good

agreement with the broad band X, which should be due to two overlapping features. The broad nature of this band is consistent with the geometry changes between the anion and neutral ground state and the dissociative nature of the $^1A'$ state.

Using Eq. (2) with the two reference energies $[E_{tot}(A,^3A'') - E_{tot}(A,^2A'')] = 4.69$ eV and $[E_{tot}(A,^1A') - E_{tot}(A,^2A'')] = 5.17$ eV, we estimated VDE's from other valence MO's: $23a'$ ($^1A'$)–5.60 eV, $9a''$ ($^3A'$)–5.45 eV, $9a''$ ($^1A'$)–5.66 eV, $22a'$ ($^3A'$)–6.21 eV, $22a'$ ($^1A''$)–6.37 eV, $8a''$ ($^3A'$)–6.21 eV, $8a''$ ($^1A'$)–6.45 eV. The 5.45 eV detachment energy from the $9a''$ orbital is in excellent agreement with the A band at 5.33 eV. The $22a'$ and $8a''$ orbitals are degenerate and the 6.21 eV detachment energies from these two MO's are in good agreement with the B band at 6.08 eV. The large number of transitions closely spaced in energy is consistent with the complicated PES spectrum observed for CrO$_5^-$.

F. Adiabatic electron affinities

The experimental and theoretical adiabatic electron affinities of the chromium oxides are summarized in Table III. The theoretical EA's computed according to Eq. (3) are: 1.17 eV (CrO),[29] 2.22 eV (CrO$_2$),[30] 3.38 eV (CrO$_3$), 4.61 eV (CrO$_4$), and 4.41 eV (CrO$_5$). These computational data are in good agreement with the experimental values. The EA's increase with the number of O atoms and saturate at CrO$_4$. This trend is consistent with our previous observations of other oxide species and indicates a sequential oxidation of the Cr atom. Both CrO$_4$ and CrO$_5$ possess rather large EA's exceeding that of atomic Cl (3.62 eV)[48] and formally belong to the class of superhalogen compounds.[49] The reason of such high EA's for the $3d$ TM oxides was first proposed on the basis of calculations by an Xα-method.[50] Our recent calculations[26,27] of FeO$_4$ and FeO$_4^-$ by the BPW91 method confirmed that the reason is in the structure of the topmost MO, which accepts the extra electron. This MO is almost entirely composed of oxygen AO's and is bonding with respect to oxygens. Note that the classical superhalogen MnO$_4$ has the A_{ad} of 4.96 eV computed at the BPW91/6-311+G* level of theory, in good agreement with the experimental value of 4.8 eV obtained from the PES spectra of MnO$_4^-$.[25] The topmost MO of MnO$_4$ is a pure oxygen one as is required by the superhalogen theory.[49]

G. Fragmentation patterns

Table IV reports the fragmentation energies of CrO$_n^-$ and CrO$_n$ computed according to Eq. (4). Experimental data are available for CrO and CrO$_2$,[51,52] and they are in fair agree-

J. Chem. Phys., Vol. 115, No. 17, 1 November 2001

Electronic structure of chromium oxides   7943

TABLE IV. Fragmentation energies (D_e in eV) of CrO_n and CrO_n^-, computed according to Eq. (4).

CrO$_n$		CrO$_n^-$	
Channel	De	Channel	De
$CrO \rightarrow Cr+O$	4.94[a]	$CrO^- \rightarrow CrO + e$	1.17
		$\rightarrow Cr + O^{-1}$	4.78
$CrO_2 \rightarrow Cr + O_2$	5.11	$CrO_2^- \rightarrow CrO_2 + e$	2.22
$\rightarrow CrO + O$	5.98[b]	$\rightarrow CrO^- + O$	6.11
		$\rightarrow Cr + O_2^-$	6.22
$CrO_3 \rightarrow CrO + O_2$	5.48	$CrO_3^- \rightarrow CrO_3 + e$	3.35
$\rightarrow CrO_2 + O$	5.31	$\rightarrow CrO_2^- + O$	6.44
		$\rightarrow CrO^- + O_2$	7.66
$CrO_4 \rightarrow CrO_2 + O_2$	2.42	$CrO_4^- \rightarrow CrO_4 + e$	4.56
$\rightarrow CrO_3 + O$	2.94	$\rightarrow CrO_3^- + O$	4.15
		$\rightarrow CrO_2^- + O_2$	4.76
$CrO_5 \rightarrow CrO_3 + O_2$	0.49	$CrO_5^- \rightarrow CrO_5 + e$	4.41
$\rightarrow CrO_4 + O$	3.37	$\rightarrow CrO_3^- + O_2$	1.55
		$\rightarrow CrO_4^- + O$	3.22

[a]Experimental D_0 value is 4.78 ± 0.09, see Ref. 51.
[b]Experimental D_0 value is $5.47^{-0.3}_{+0.65}$, see Ref. 52.

ment with our computational results. Since Cr has a $4s^1 3d^5$ electronic configuration, it has a formal valence of six. However, the Cr–O bond is stronger in CrO_2 than that in CrO_3 in contrast to the anticipation based on the notion of maximum saturation of formal vacancies. CrO_4 is stable by about 55 kcal/mol while CrO_3 is stable by only 10 kcal/mol toward evolution of molecular oxygen.

The low-energy decay channels of CrO_n^- anion correspond to detachment of an extra electron for $n=1-3$. CrO_4^- is almost equally stable toward detachment of an extra electron or dissociation of atomic and molecular oxygen. While CrO_3^- is rather stable towards detachment of an extra electron and dissociation of an atomic oxygen, it is much less stable toward evolution of molecular oxygen, as would be expected due to the superoxo O_2 bonding in CrO_5^-.

V. SUMMARY

We report a comprehensive theoretical and experimental investigation of CrO_n^- ($n=1-5$) and their corresponding neutral species. Photodetachment photoelectron spectra were obtained for the anions produced from a laser vaporization cluster source at various photon energies. Calculated adiabatic and vertical binding energies of CrO_n^- are in good agreement with the experimental values. We show that theoretical calculations are very helpful in interpretations of the photoelectron spectra of the anions, in understanding the electronic and geometrical structures of their ground and excited states, and chemical bonding for both the anions and the neutral species.

ACKNOWLEDGMENTS

[1] H. H. Kung, *Transition Metal Oxides: Surface Chemistry and Catalysis* (Elsevier, New York, 1989).
[2] P. C. Thune, R. Linke, W. J. H. van Gennip, A. M. de Jong, and J. W. Niemantsverdriet, J. Phys. Chem. B **105**, 3073 (2001).
[3] H. Brandle, D. Weller, S. S. Parkin et al., Phys. Rev. B **46**, 13889 (1992).
[4] M. A. Korotin, V. I. Anisimov, D. I. Khomskii, and G. A. Sawatzky, Phys. Rev. Lett. **80**, 4305 (1998).
[5] C. W. Walter, C. F. Hertzeler, P. Devynck, G. P. Smith, and J. R. Peterson, J. Chem. Phys. **95**, 824 (1991).
[6] E. B. Rudnyi, O. M. Vovk, and E. A. Kaibicheva, J. Chem. Thermodyn. **21**, 247 (1989).
[7] H. Wu, S. R. Desai, and L. S. Wang, J. Chem. Phys. **103**, 4363 (1995).
[8] H. Wu, S. R. Desai, and L. S. Wang, J. Am. Chem. Soc. **118**, 5296 (1996).
[9] H. Wu, S. R. Desai, and L. S. Wang, J. Phys. Chem. **101**, 2103 (1997).
[10] H. Wu and L. S. Wang, J. Chem. Phys. **107**, 16 (1997).
[11] L. S. Wang, H. Wu, and S. R. Desai, Phys. Rev. Lett. **76**, 4853 (1996).
[12] L. S. Wang, H. Wu, S. R. Desai, J. Fan, and S. D. Colson, J. Phys. Chem. **100**, 8697 (1996).
[13] L. S. Wang, *Photodetachment Photoelectron Spectroscopy of Transition Metal Oxide Species*, in Advanced Series in Physical Chemistry, Photoionization and Photodetachment, Vol. 10, edited by C. Y. Ng (World Scientific, Singapore, 2000), p. 854.
[14] G. L. Gutsev, B. K. Rao, P. Jena, X. Li, and L. S. Wang, J. Chem. Phys. **113**, 1473 (2000).
[15] P. G. Wenthold, R. F. Gunion, and W. C. Lineberger, Chem. Phys. Lett. **258**, 101 (1996).
[16] P. G. Wenthold, K.-L. Jonas, and W. C. Lineberger, J. Chem. Phys. **106**, 9961 (1997).
[17] P. C. Engelking and W. C. Lineberger, J. Chem. Phys. **66**, 5054 (1977).
[18] T. Andersen, K. R. Lykke, D. M. Neumark, and W. C. Lineberger, J. Chem. Phys. **86**, 1858 (1987).
[19] R. F. Gunion, S. J. Dixon-Warren, W. C. Lineberger, and M. D. Morse, J. Chem. Phys. **104**, 1765 (1996).
[20] C. W. Bauschlicher, Jr., M. Zhou, L. Andrews, J. R. T. Johnson, I. Panas, A. Snis, and B. O. Roos, J. Phys. Chem. **103**, 5463 (1999).
[21] M. Rosi, C. W. Bauschlicher, Jr., G. V. Chertihin, and L. Andrews, Theor. Chem. Acc. **99**, 106 (1998).
[22] G. V. Chertihin, L. Andrews, M. Rosi, and C. W. Bauschlicher, Jr., J. Phys. Chem. **101**, 9085 (1997).
[23] M. B. Walsch, R. A. King, and H. F. Schaefer III, J. Chem. Phys. **110**, 5224 (1999).
[24] S. F. Vyboishchikov and J. Sauer, J. Phys. Chem. A **104**, 10913 (2000).
[25] G. L. Gutsev, B. K. Rao, P. Jena, X. B. Wang, and L. S. Wang, Chem. Phys. Lett. **312**, 598 (1999).
[26] G. L. Gutsev, B. K. Rao, and P. Jena, J. Phys. Chem. A **103**, 10819 (1999).
[27] G. L. Gutsev, S. N. Khanna, B. K. Rao, and P. Jena, Phys. Rev. A **59**, 3681 (1999).
[28] G. L. Gutsev, S. N. Khanna, B. K. Rao, and P. Jena, J. Phys. Chem. **103**, 5812 (1999).
[29] G. L. Gutsev, B. K. Rao, and P. Jena, J. Phys. Chem. A **104**, 5374 (2000).
[30] G. L. Gutsev, B. K. Rao, and P. Jena, J. Phys. Chem. A **104**, 11961 (2000).
[31] A. D. Becke, Phys. Rev. A **38**, 3098 (1988).
[32] J. P. Perdew and Y. Wang, Phys. Rev. B **45**, 13244 (1991).
[33] C. Lee, W. Yang, and R. G. Parr, Phys. Rev. B **37**, 785 (1988).
[34] A. D. Becke, J. Chem. Phys. **98**, 5648 (1993).
[35] L. S. Wang, H. S. Cheng, and J. Fan, J. Chem. Phys. **102**, 9480 (1995).
[36] L. S. Wang and H. Wu, in *Advances in Metal and Semiconductor Clusters. IV. Cluster Materials*, edited by M. A. Duncan (JAI, Greenwich, CT, 1998), p. 299.
[37] M. J. Frisch, G. W. Trucks, H. P. Schlegel et al., GAUSSIAN 94, Revision B.1, Pittsburgh, PA.
[38] A. J. H. Wachters, J. Chem. Phys. **52**, 1033 (1970).
[39] P. J. Hay, J. Chem. Phys. **66**, 4377 (1977).
[40] W. Kohn and L. J. Sham, Phys. Rev. A **140**, 1133 (1965).
[41] O. Gunnarsson and B. I. Lundqvist, J. Chem. Phys. **13**, 4274 (1976).
[42] E. K. U. Gross, L. N. Oliveira, and W. Kohn, Phys. Rev. A **37**, 2809 (1988).
[43] A. Gorling, S. B. Trickey, P. Gisdakis, and N. Rosh, *Topics in Organome-

tallic Chemistry, edited by P. Hoffman and J. M. Brown (Springer, New York, 1999), Vol. 4, pp. 109–165.

[44] S. Veliah, K.-H. Xiang, R. Pandey, J. M. Recio, and J. M. Newsam, J. Phys. Chem. **102**, 1126 (1998).

[45] G. V. Chertihin, W. D. Bare, and L. Andrews, J. Chem. Phys. **107**, 2798 (1997).

[46] A. J. Merer, Annu. Rev. Phys. Chem. **40**, 407 (1989).

[47] K. P. Huber and G. Herzberg, *Constants of Diatomic Molecules* (Van Nostrand Reinhold, New York, 1979).

[48] H. Hotop and W. C. Lineberger, J. Phys. Chem. Ref. Data **14**, 731 (1985).

[49] G. L. Gutsev and A. I. Boldyrev, Adv. Chem. Phys. **61**, 169 (1985).

[50] G. L. Gutsev and A. I. Boldyrev, Chem. Phys. Lett. **108**, 255 (1984).

[51] H. Kang and J. L. Beauchamp, J. Am. Chem. Soc. **108**, 5663 (1986).

[52] R. T. Grimley, R. P. Burns, and M. Inghram, J. Chem. Phys. **34**, 664 (1961).